applied sciences

MDPI

Article

Virtual Space-Time DiversityTurbo Equalization Using Cluster Sparse Proportional Recursive Least Squares Algorithm for Underwater Acoustic Communications

Zhen Han [1], Weiliang Tao [2], Dan Zhang [3] and Peng Jiang [1,*]

[1] GNSS Research Center, Wuhan University, Wuhan 430072, China; willhanzhen@whu.edu.cn
[2] Electronic Information School, Wuhan University, Wuhan 430072, China; taoweiliang@whu.edu.cn
[3] School of Computer Science, Wuhan University, Wuhan 430079, China; zhangxiaobei125@whu.edu.cn
* Correspondence: jiangp@whu.edu.cn

Abstract: The oceanic positioning, navigation and timing (PNT) network requires high-quality underwater acoustic message transmission. Turbo equalization technology has exhibited superior performance for underwater acoustic (UWA) communications compared with conventional channel equalizers. To overcome the performance reduction caused by severe doubly selective UWA channels, the virtual space-time diversity soft direct-adaptation turbo equalization is proposed for UWA communications. The proposed scheme improves the ability of the typical turbo equalizer to deal with both Doppler and multipath effects for time varying channels. We utilize a fractionally spaced soft interference cancellation equalizer (FS-SE) instead of a hard decision to constitute the soft-input soft-output (SISO) equalizer. Combined with another virtual time-reversal mirror equalizer component, we can obtain virtual space and time diversity with only a single receiving transducer and mitigate the error propagation phenomenon of the feedback filter. To satisfy the sparse UWA channel, the $\ell_{p,q}$-PRLS algorithm is applied to adaptive updates for FS-SE. In the proposed scheme, an adjustable interpolator and digital phase-locked loop are embedded into the equalizer to overcome the residual Doppler frequency shift and recover the timing distortion. Results of simulations and field lake trial show that the proposed scheme achieves better performance than existing ones under the same equalizer order.

Keywords: underwater acoustic communications; turbo equalization; PRLS

check for updates

Citation: Han, Z.; Tao, W.; Zhang, D.; Jiang, P. Virtual Space-Time Diversity Turbo Equalization Using Cluster Sparse Proportional Recursive Least Squares Algorithm for Underwater Acoustic Communications. *Appl. Sci.* **2023**, *13*, 11050. https://doi.org/10.3390/app131911050

Academic Editor: Atsushi Mase

Received: 11 September 2023
Revised: 4 October 2023
Accepted: 5 October 2023
Published: 7 October 2023

1. Introduction

The oceanic positioning, navigation and timing (PNT) network has recently become a promising major underwater infrastructure and will eventually play a crucial part in marine development and utilization [1]. Underwater acoustics (UWAs), which are still the only efficient wireless signal for long-range transmission in the sea, will be exploited to provide interaction and location information for underwater vehicles or users, e.g., remotely operated vehicles (ROVs) and autonomous underwater vehicles (AUVs). The UWA communication, navigation and detection integration system (UCNDIS) [2] is gradually regarded as the prospective solution to the implementation of the oceanic PNT network. Loosely coupled UCNDISs consist of multiple acoustic devices with different functions, e.g., a UWA communication modem, an ultra-short base line (USBL) system and so on, to achieve functional integration. Obviously, the loosely coupled UCNDIS commonly has some drawbacks, such as hardware waste, high power consumption and high processing delay. Then, tightly coupled UCNDISs, which are able to satisfy all PNT demands simultaneously by reusing the same hardware platform, are increasingly attracting researchers' attention [3]. One route for tightly coupled UCNDISs is to obtain position and timing information based on communication signals [4], making high-quality and robust

UWA communication technology the foundation for the implementation of tightly coupled UCNDISs.

The performance of underwater acoustic communication is extremely affected by time-varying transmission channels [5]. Owing to its abominable propagation characteristics, such as a low speed of the acoustic signal, large attenuation and significant multipath interference, the UWA channel can be seen as one of the most challenging elements [6]. The Doppler effect and multipath propagation caused by boundary reflection are the fundamental factors causing channel distortion, for which the acoustic signal experiences time and frequency selectivity [7–9]. One of the most widely utilized approaches to mediate harsh inter-symbol interference (ISI) due to channel aberration is the use of a decision-feedback equalizer (DFE) with a digital phase locked loop (DPLL) embedded in it [10].

Traditional time-domain equalizers cannot satisfy the requirements of precise information, especially in high-speed UWA communications of shallow water nowadays. Turbo equalization has been considered as an efficient technology to make significant improvements in bit error rate (BER) manifestation under complicated UWA environments [11,12]. Turbo equalization is derived from turbo decoders by employing a maximum a posteriori (MAP) equalizer as a replacement of one stand-alone MAP decoder in typical decoder processing [13,14]. In order to realize computational complexity in large time-delay channels, a soft-input soft-output (SISO) equalizer is introduced into the iteration structure based on the minimum mean squared error (MMSE) criterion [15–17], least symbol error rate (LSER) criterion [18,19] and so on. In some scenarios of high SNR, the adaptive equalizers based on the LSER criterion achieve better BER performance than the MMSE. The chief drawback of traditional DFEs is the error propagation of the feedback filter when extensive, inaccurate hard-decision symbols occur. A usually efficient method is the exploitation of a soft-decision feedback equalizer instead of a hard-decision one [15]. Another neoteric method is the bidirectional structure of an equalizer, which accomplishes the target of eliminating error propagation through a normal SISO equalizer and a time-reversed one using the virtual time reversal mirror (VTRM) technique [18,20,21]. The TRM technology with a simple structure provides noise suppression for communication systems equipped with single or multiple receiving transducers. Fractionally spaced equalizers (FSEs) have been applied in normal one-iteration channel equalization successfully for years and can achieve channel diversity gain by increasing the baseband sampling frequency to several times the symbol rate [22]. The several branches are regarded as independently identical distributions when the FS order is low enough. However, the FSE has seldom been employed for turbo equalization in current works, and researchers have exhibited more interest in multiple receivers to achieve space diversity [23–25].

Turbo equalization applied to UWA communications is classified into two categories depending on whether channel estimation is carried out or not. The channel-estimation-based turbo equalization (CE-TEQ) has to compute the equalizer coefficients, which involve a large-dimension matrix inversion, particularly in the long-time delay-spread channel [25,26]. Moreover, because the UWA channel is time-varying, repetitive channel estimation would be an encumbrance to computation. Without redundant channel estimations, direct-adaptation-based turbo equalization (DA-TEQ) commonly implements suboptimal performance by disposing of adaptive filtering and gradually converges equalizer taps. Recently, a soft DA-TEQ (SDA-TEQ) has been proposed, and the significant innovation is that the data source of the feedback filter (FBF) is the a priori soft decisions of the MAP decoder instead of hard-decision symbols, which accelerates the convergence rate of iterations and eliminates the error propagation of hard detections [15,16].

In recent research works, the SISO equalizer adaptive algorithms of UWA TEQs concentrated on the least mean square (LMS) category. In [15], a DA-TEQ with an improved proportional normalized LMS (IPNLMS) algorithm used in a multi-input multi-output (MIMO) system shows BER and MMSE performance improvements compared to NLMS. In [27], the researchers developed sparsity-aware IPNLMS adapted in DA-TEQ for a sparse UWA channel. In [16], the fast self-optimized LMS (FOLMS) algorithm embedded in

Soft-DA-TEQ is proposed, and experiments show a faster convergence rate than Hard DA-TEQ. Recursive least-squares (RLS) adaptive algorithms have exhibited tremendously faster convergence in situations of longer channel taps in comparison with LMS category algorithms [28–30]. In [31], a CE-TEQ scheme for MIMO system with a low-complexity homotopy RLS algorithm is proposed, and lake trial results demonstrate the superiority of the RLS-type algorithm could achieve promising detection performance, while the IPNLMS-based scheme cannot obtain a satisfactory manifestation. Recently, the proportional RLS (PRLS) algorithm [32] has been proposed and exhibits superior performance over conventional RLS for both UWA channel estimation and equalization problems [28,33].

In this paper, motivated by the work in [15,16,34], we propose a bidirectional soft direct-adaptation-based turbo equalization for SISO UWA communication systems. In comparison to existing works, the improvements of the proposed scheme are summarized as follows.

First, the proposed scheme, namely virtual space-time diversity turbo equalization (VSTD-TEQ), integrates a fractionally spaced soft interference cancellation equalizer (FS-SE) and a time-reversed FS-SE. Attributed to the low correlation between the soft outputs of the bidirectional equalizer, the virtual time diversity gain would alleviate error propagation. Furthermore, a fractionally spaced structure can exploit the virtual space diversity gain in SISO systems and mitigate wrong decision symbols effectively.

Second, an interpolator is inserted into VSTD-TEQ, which accomplishes the Doppler effect dislodgement together with a DPLL, especially in the circumstance that evolves a higher residual Doppler frequency shift due to low-resolution Doppler search gap or dynamic Doppler phenomenon. The main function of the interpolator is to mitigate the accumulated sampling timing error of the baseband caused by Doppler motion in a harsh ISI channel.

Third, the PRLS algorithm is modified using mixed-norm regularization to satisfy the cluster sparse UWA channel.

For the sake of clarity, all of the abbreviations used in this paper are summarized in the Abbreviation section.

2. System Model

The time-varying UWA channel impulse response (CIR) can be demonstrated as the superposition of propagation multipaths with the Doppler effect. The time-domain CIR with N_p discrete multipaths is given as [8]:

$$h(t,\tau) = \sum_{i=1}^{N_p} A_i(t)\delta(\tau - (\tau_i - \alpha_i(t)t)) \tag{1}$$

where $A_i(t)$ and τ_i are the time-varying amplitude and initial time delay of the i-th path, α_i is the Doppler factor of the i-th path. For the shallow-water UWA communication scenario, where the horizontal transmission distance is much further than the vertical direction, the Doppler factor of multipaths is approximately the same [35,36], i.e., $\{\alpha_i(t)\}_{i=1}^{N_p} = \alpha(t)$. Furthermore, assuming that the channel is slow time-varying, we can suppose that $A_i \leftarrow A_i(t)$ and $\alpha_i \leftarrow \alpha_i(t)$ are invariant during observation. Considering a single-carrier UWA communication system, the passband received signal of hydrophone is given as [30]:

$$y(t) = \sum_{i=1}^{N_p} A_i \tilde{x}((1+\alpha)t - \tau_i) + v(t) \tag{2}$$

where $\tilde{x}(t) = \sum_{n=1}^{N} \tilde{x}_n(t)$ is the transmitted signal of source, N is the length of baseband sequence, $v(t) \sim \mathcal{N}(0, \sigma_v^2)$ is the additive white Gaussian noise (AWGN).

2.1. Cluster Sparse UWA Channel

For time instant n, the discrete CIR $\mathbf{h}(n) = [h_1(n), h_2(n), \ldots, h_N(n)]^T \in \mathbb{C}^N$of UWA channel with standard sparse characteristic follows a Bernoulli-Complex Gaussian (B-CG) distribution [26], as:

$$p(h_n) = \varsigma \mathcal{CN}(h_n; \mu_h, \sigma_h^2) + (1 - \varsigma)\delta(h_n) \tag{3}$$

where μ_h, σ_h^2 are the mean and variance of the non-zero taps, respectively, ς is the channel sparsity, $\delta(\cdot)$ is the Dirac function. Recent research has shown that the propagation paths of sparse UWA channel appear in several distinct clusters [37]. The cluster sparse CIR is constructed as the time-domain superposition of finite clusters, as:

$$\mathbf{h}(n) = \sum_{i=1}^{C} \mathbf{h}_{\mathbf{\Psi}_i}(n) \tag{4}$$

where C is the cluster number, and $\{\mathbf{\Psi}_i\}_{i=1}^{C}$ is the subset of the index set of CIR vector taps $\mathbf{\Psi} = \{1, 2, \cdots, N\}$ and satisfies the following relationship:

$$\begin{gathered} \bigcup_{i=1}^{C} \mathbf{\Psi}_i = \mathbf{\Psi} \\ \mathbf{\Psi}_i \bigcap \mathbf{\Psi}_j = \varnothing, \text{when} \quad i \neq j \end{gathered} \tag{5}$$

If the subset of CIR $\mathbf{h}_{\mathbf{\Psi}_i}(n)$ contains any non-zero tap, $\mathbf{h}_{\mathbf{\Psi}_i}(n)$ will follow the B-CG distribution corresponding to its index vector $\mathbf{\Psi}_i$:

$$\begin{cases} h_{\mathbf{\Psi}_i,k} \sim \text{B-}\mathcal{CN}(\mu_i, \sigma_i^2, \varsigma_i), & \|\mathbf{h}_{\mathbf{\Psi}_i}\|_1 \neq 0 \\ \mathbf{h}_{\mathbf{\Psi}_i} = \mathbf{0}_{\mathbf{\Psi}_i}, & \text{else} \end{cases} \tag{6}$$

where $h_{\mathbf{\Psi}_i,k}$ is the k-th element of $\mathbf{h}_{\mathbf{\Psi}_i}$.

2.2. Transmitted Signal Pattern

A single carrier phase shift keying (PSK) modulation with channel coding is taken into consideration here. For the k-th frame transmitted signal, the bit stream $\mathbf{b}_k$ of baseband is first encoded by a recursive system convolutional (RSC) decoder and interleaved by a random interleaver, and the size of produced binary bit stream $\mathbf{c}_k$ is generally different from $\mathbf{b}_k$. Assuming that a q-order modulation is exploited, the symbol constellation contains 2^q pots, i.e., the constellation set $S = \{\gamma_1, \cdots, \gamma_{2^q}\}$. The relevant bit pattern of the constellation pot γ_i is $s_i = [s_i^1, \cdots, s_i^q]$, where $s_i^q \in \{+1, -1\}$. Then, $\mathbf{c}_k$ is divided into segments according to the adjacent q bits with $\mathbf{c}_{k,n} = [c_{k,n}^1, \cdots, c_{k,n}^q]$. Finally, the grouped bits are mapped to the constellation, resulting in the transmitted baseband signal $\mathbf{x}_k$. Under the assumption that the correlation between neighbouring frames is independent, we omit the subscript character k. Therefore, the passband transmitted signal of the n-th symbol is given as [38]:

$$\tilde{x}_n(t) = \Re\{x_n \exp\{j2\pi f_c t\} g(t - nT_c)\} \tag{7}$$

where $\mathbf{x} = [x_1, \cdots, x_n, \cdots, x_N]^T$, f_c is the carrier frequency, $g(t)$ is the pulse shaping filter, T_c is the symbol period. For flatness in passband, the raised cosine rolling-off shaping filter is commonly used in UWA communication systems due to the severe frequency selective fading.

2.3. Discrete Received Signal Pattern

The passband signal in Equation (7) transferred through the doubly selective UWA channel is sampled into the receiver by an analog to digital converter (ADC). Corresponding to the model in Equation (2), the discrete received signal is given as [39]:

$$\tilde{y}(n) = \Re\left\{\sum_{i=1}^{N_p}\sum_{n=1}^{N} A_i x_n \exp\left\{j2\pi\frac{n}{\kappa_c}((1+\alpha)\frac{n}{f_s} - n_{\tau_i})\right\} g((1+\alpha)\frac{n}{f_s} - n_{\tau_i} - n\kappa_b)\right\} + v(\frac{n}{f_s}) \tag{8}$$

where $n_{\tau_i} = \tau_i f_s$, $\kappa_c = f_s/f_c$, $\kappa_c = f_s/R_b$, R_b is the symbol rate, f_s is the sampling frequency of ADC.

3. Virtual Space-Time Diversity Turbo Equalization

The proposed virtual space-time diversity SDA-TEQ (VSTD-TEQ) for SISO UWA communication systems is demonstrated in Figure 1. To exert plenitudinous performance of single carrier system for the data accuracy demand of oceanic PNT, we integrated Soft FS-SE with an anti-Doppler module, time-reversal bidirectional processing and turbo equalization technology systematically into the proposed scheme. The parameters are adaptively updated based on PRLS-type algorithms. The red line in Figure 1 represents the input and output of the adaptive updating scheme, the black line represents the signal flow, and the blue line represents the feedback signal. The meanings of the parameters in Figure 1 have been stated in related sections. Symbols $\otimes$ and $\oplus$ represent the multipliers and adders, respectively.

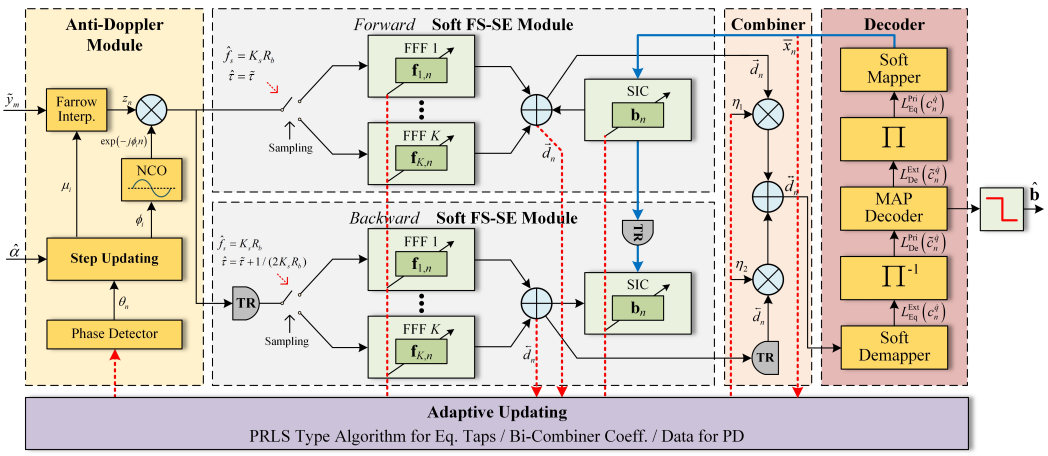

Figure 1. Structure of the proposed VSTD-TEQ for UWA communication systems.

3.1. FS-SE with Anti-Doppler Module

The time-domain channel equalizer structure, as shown in Figure 2, is a loop-locked scheme to overcome the fast time-varying Doppler effect. The loop-locked anti-Doppler time-domain channel equalizer consists of an anti-Doppler module (ADM) and a fractionally spaced soft interference cancellation (SIC)-based equalizer (FS-SE) module. The ADM utilizes an adjustable scheme to solve the dynamic residual Doppler effect of the individual frame. The FS-SE module is exploited to eliminate ISI.

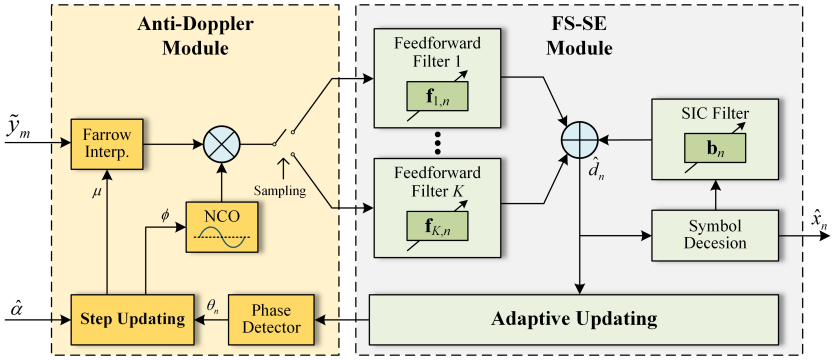

Figure 2. Anti-Doppler time-domain channel equalizer.

A two-step method is exploited to accomplish Doppler spread compensation. The original dominant Doppler spread of the received signal is first compensated by a Farrow structure interpolator. Assuming that the main Doppler factor estimated by synchronizing the signal through the matched filtering techniques is $\hat{\alpha}$ and the total Doppler factor estimate is μ, the main time-domain spread caused by the Doppler effect of the received signal is compensated with an interpolator. Without losing generality, we adopt Lagrange interpolation (N-segment M-order polynomial) with Farrow structure [40] in this work. After down conversion, the frontforward input of FS-SE is given as follows

$$z_n = \sum_{i=0}^{M}\sum_{j=0}^{N} \frac{\tilde{y}_{m_n - j c_{i,j}}}{(1+\mu)^i} \exp\{-j2\pi f_c (kT_c/K_s + \tilde{\tau})\} \tag{9}$$

where $c_{i,j}$ is the coefficient of the interpolator, m_n is the floor integer index of resampling time instant, $\tilde{\tau}$ is the time delay of frame synchronization. The FS-SE contains K_s-order parallel feedforward filters (FFFs) and a SIC filter for compensation of the linear characteristics of the UWA channel. According to the order of fractional space [34], z_n is downsampled and allocated to K_s FFFs. The output of FS-SE is given as

$$\hat{d}_n = \sum_{k=1}^{K_s} \mathbf{f}_{k,n}^H \mathbf{z}_{k,n} e^{-j\hat{\varphi}_n} - \mathbf{b}_n^H \bar{\mathbf{x}}_n \tag{10}$$

where the length of FFF $\mathbf{f}_{k,n}$ is $N_{f,1} + N_{f,2} + 1$, the length of SIC is $N_{b,1} + N_{b,2} + 1$. $\mathbf{z}_{k,n} = [z_{k,n+N_{f,1}}, \cdots, z_{k,n-N_{f,2}}]^T$ and $\bar{\mathbf{x}}_n = [\bar{x}_{n-N_{b,1}}, \cdots, \bar{x}_{n-1}, 0, \bar{x}_{n+1}, \cdots, \bar{x}_{n+N_{b,2}}]^T$ are the inputs of k-th FFF and SIC, respectively. $\hat{\varphi}_k$ is the phase compensation of DPLL. Especially, the SIC will degenerate into the normal feedback filter of the decision-feedback equalizer when $N_{b,2} = 0$. The FS-SE output using combined taps is rewritten as

$$\hat{d}_n = \mathbf{w}_n^H \mathbf{u}_n \tag{11}$$

where $\mathbf{w}_n = [\mathbf{f}_{1,n}^T e^{-j\hat{\varphi}_n}, \cdots, \mathbf{f}_{K_s,n}^T e^{-j\hat{\varphi}_n}, -\mathbf{b}_n^T]^T$,$\mathbf{u}_n = [\mathbf{z}_{1,n}^T, \cdots, \mathbf{z}_{K_s,n}^T, \bar{\mathbf{x}}_n^T]^T$, and their lengths are both $N_{eq} = K_s(N_{f,1} + N_{f,2} + 1) + N_{b,1} + N_{b,2} + 1$. The adaptive update of $\mathbf{w}_n$ will be discussed in the following section.

The residual Doppler effect contributes to phase rotation of the FS-SE input signal. We can obtain the instantaneous phase error of the equivalent phase detector (PD) [41,42]:

$$\theta_n = \Im\{p_n(x_n + q_n)\} \approx \Im\left\{\hat{d}_n x_n^*\right\} \tag{12}$$

where $p_n = \sum_{k=1}^{K_s} \mathbf{f}_{k,n}^H \mathbf{z}_{k,n} e^{-j\hat{\varphi}_n}$, $q_n = \mathbf{b}_n^H \bar{\mathbf{x}}_n$. Assuming $\mathbb{E}[p_n q_n^*] = 0$, we can obtain Equation (12) by avoiding the calculation of p_n and q_n. The expression of Equation (12) is similar to the phase estimate result in [43]. In the tracking stage of equalizer, x_n in Equation (12) is replaced by $Q[\hat{d}_n]$, the estimate produced by the decision function. Figure 3 shows the step updating diagram for ADM. The instantaneous θ_n generally contain serious

noise and cannot be used for numerically controlled oscillator (NCO) control directly. We introduce the integral-zeroing module, a lowpass filter (LPF), for high-frequency noise cancellation. The output of the integral-zeroing module is given as

$$\bar{\theta}_i = \frac{1}{N_k} \sum_{n=(i-1)N_k}^{iN_k-1} \theta_n \tag{13}$$

where i and N_k are the index and period of carrier NCO update, respectively. The step of the carrier NCO is changed every N_k symbol period. Generally, N_k is in direct proportion to the length of the AD sampling block in our design. We utilize the collected data in a 200 m horizontal range lake trial to verify the performance of the integral-zeroing module. Figure 4 is the comparison of phase detectors, and the integral-zeroing module performs superiorly. The processed $\bar{\theta}_i$ is obviously smoother than θ_n and able to reflect the true phase error better.

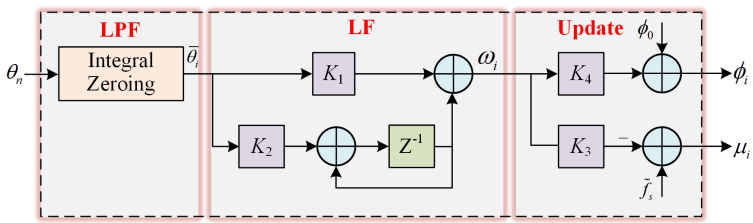

Figure 3. Step updating diagram.

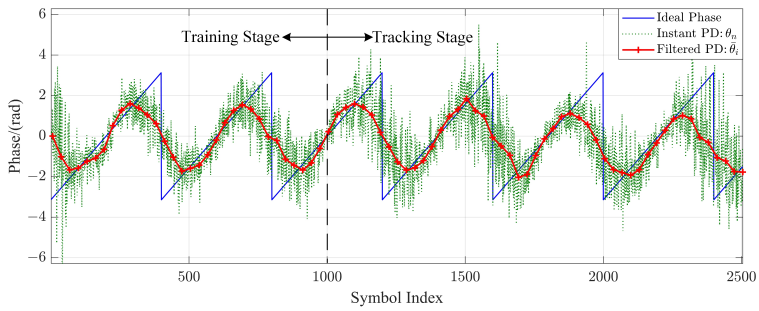

Figure 4. Result comparisons of phase detectors.

Then, $\bar{\theta}_i$ is sent to the one-order loop filter (LF), and the Doppler factor estimate and carrier NCO step are updated as:

$$\begin{aligned} \omega_i &= (K_1 + K_2)\bar{\theta}_i - K_1\bar{\theta}_{i-1} + \omega_{i-1} \\ \phi_i &= \phi_0 + \frac{\omega_i \pi}{2^{M_{\mathrm{NCO}}}} \\ \mu_i &= \tilde{f}_s - K_3\omega_i \end{aligned} \tag{14}$$

where ω_i is the output of LF, K_1 and K_2 are the parameters of LF, ϕ_i and $\phi_0 = 2\pi f_c / f_s$ are the updated step and initial step of carrier NCO, respectively. M_{NCO} is the order of carrier NCO, μ_i is the resampling frequency of interpolator, $\tilde{f}_s = f_s/(1+\hat{\alpha})$ and K_3 is a scaling factor. Moreover, K_4 in Figure 3 is given as $K_4 = \pi/2^{M_{\mathrm{NCO}}}$ for simplification.

3.2. Cluster Sparse $\ell_{p,q}$-PRLS Adaptive Filtering Algorithm

The update of equalizer coefficients $\mathbf{w}_n$ can be regarded as an adaptive filtering process. Under the condition of sparsity and zero-attracting principle, a penalty item should be added into the RLS cost function to satisfy the cluster sparse UWA channel. The modified cost function is given as [32]:

$$J[\mathbf{w}_n] = J_{\mathrm{RLS}}[\mathbf{w}_n] + J_{p,q}[\mathbf{w}_n] \tag{15}$$

where the $\ell_{p,q}$-norm penalty item is defined as [44]:

$$J_{p,q}[\mathbf{w}_n] \triangleq \gamma \left(\sum_{j=1}^{C} \|\mathbf{w}_{\mathbf{\Psi}_i,n}\|_p^q \right)^{q^{-1}} \tag{16}$$

$\gamma \in \mathbb{R}^+$ is the regularization factor. Therefore, the $\ell_{p,q}$-RLS algorithm is derived by minimizing the modified cost function $J[\mathbf{w}_n]$ in Equation (15). Item $J_{p,q}[\mathbf{w}_n]$ may be a non-differentiable convex function or a non-convex function; therefore, a subgradient analysis is introduced to replace the gradient of the objective function. The subgradient of $J_{p,q}[\mathbf{w}_n]$, with respect to $\mathbf{w}_n$, is denoted by $\nabla^s J_{p,q}[\mathbf{w}_n]$.

We can derive the $\ell_{p,q}$-PRLS algorithm, which utilizes the proportionate updating matrix, to control the adjustments caused by the Kalman gain vector of the $\ell_{p,q}$-RLS. The proposed $\ell_{p,q}$-PRLS algorithm is expressed as follows:

$$\mathbf{w}_n = \mathbf{w}_{n-1} + \mathbf{G}_{n-1}\mathbf{k}_n e_n^* - \hat{\gamma}\nabla^s J_{p,q}[\mathbf{w}_{n-1}] \tag{17}$$

where $\mathbf{G}_n$ is the $N_{eq} \times N_{eq}$ diagonal proportionate matrix, and its i-th diagonal entry $g_{n,i}$ is calculated as [28,33]:

$$g_{n,i} = \begin{cases} \dfrac{\tau_1(1-\beta_1)}{2N} + \dfrac{\tau_1(1+\beta_1)|w_{n,i}|}{2\|\mathbf{w}_n\|_1 + \epsilon_g} & i \in [1, K_s(N_{f,1} + N_{f,2} + 1)] \\ \dfrac{\tau_2(1-\beta_2)}{2N} + \dfrac{\tau_2(1+\beta_2)|w_{n,i}|}{2\|\mathbf{w}_n\|_1 + \epsilon_g} & i \in [K_s(N_{f,1} + N_{f,2} + 1) + 1, N_{eq}] \end{cases} \tag{18}$$

where $\{\beta_m\}_{m=1}^2 \in [-1, 1]$, $\{\tau_m\}_{m=1}^2 \in (0, N_{eq})$ is a trading off parameter and ϵ_g is a small positive constant for computational stability. Parameter $\hat{\gamma}$ is a simplified form of $\hat{\gamma} \leftarrow \gamma(1-\lambda)\mathbf{P}_n$, where β is an adjustment factor of sparse regularization, $\mathbf{P}_n$ is the inverse of the input correlation matrix. The Kalman gain vector $\mathbf{k}_n$, $\mathbf{P}_n$ and a priori error e_n are respectively given by

$$\mathbf{k}_n = \frac{\mathbf{P}_{n-1}\mathbf{u}_n}{\lambda + \mathbf{u}_n^H \mathbf{P}_{n-1}\mathbf{u}_n} \tag{19}$$

$$\mathbf{P}_n = \frac{1}{\lambda}\left(\mathbf{P}_{n-1} - \mathbf{k}_n \mathbf{u}_n^H \mathbf{P}_{n-1}\right) \tag{20}$$

$$e_n = \begin{cases} x_n - \hat{d}_n & \text{Training Stage} \\ Q[\hat{d}_n] - \hat{d}_n & \text{Tracking Stage} \end{cases} \tag{21}$$

where λ is the forgetting factor, $Q[\cdot]$ is the decision function. Several gradients or subgradients of $\ell_{p,q}$-norm penalty regularization items are listed in Table 1.

Table 1. Gradients or subgradients of some usual $\ell_{p,q}$-norm penalty regularization items.

$\{p,q\}$	$\nabla^s J_{p,q}[w_{n,i}]$
1 [1]	$\mathrm{sgn}\{w_{n,i}\}$ [3]
0 [2]	$\alpha\mathrm{sgn}\{w_{n,i}\} - \alpha^2 w_{n,i}$
$\{2,1\}$	$\sum_{j=1}^{C} \dfrac{\alpha w_{\mathbf{\Psi}_j,n,i}}{\|\mathbf{w}_{\mathbf{\Psi}_j,n}\|_2 + \epsilon_p}$ [4]
$\{2,0\}$	$\sum_{j=1}^{C} \dfrac{\alpha w_{\mathbf{\Psi}_j,n,i}}{\|\mathbf{w}_{\mathbf{\Psi}_j,n}\|_2 + \epsilon_p}\left(1 - \alpha\|\mathbf{w}_{\mathbf{\Psi}_j,n}\|_2\right)$
$\{1,0\}$	$\sum_{j=1}^{C} \alpha\mathrm{sgn}\left\{w_{\mathbf{\Psi}_j,n,i}\right\}\left(1 - \alpha\|\mathbf{w}_{\mathbf{\Psi}_j,n}\|_1\right)$

[1] ℓ_1-norm penalty. [2] ℓ_0-norm penalty. [3] $\mathrm{sgn}\{\cdot\}$ is the component-wise sign function. [4] α is an appropriate constant, ϵ_p is a small positive constant, $w_{\mathbf{\Psi}_j,n,i}$ is the i-th element of vector $\mathbf{w}_{\mathbf{\Psi}_j,n}$.

3.3. Bidirectional Combination

The virtual time-reversal mirror (VTRM) is designed to reduce the error propagation (EP) of equalizers with feedback input. The bidirectional combination scheme based on VTRM consists of two individual FS-SEs with opposite direction. The input of the backward FS-SE is time-reversed of received signal, as $\{\overleftarrow{z}_n\} \leftarrow \{z_{-n}\}$, while the input of the forward FS-SE is $\{z_n\}$. Assuming that the noise of input of the bidirectional FS-SE is independent Gaussian noise for the memoryless character of the Gaussian process, the noise of the outputs can be approximatively regarded as independent Gaussian noise. The SNR of soft symbols processed by linear bidirectional combination is improved, so that the bidirectional combination scheme can be considered as a kind of time diversity technology.

The linear combined soft symbol of the equalizer output is given as

$$\overleftrightarrow{d}_n = \eta_1 \overrightarrow{d}_n + \eta_2 \overleftarrow{d}_n \tag{22}$$

where $\mathcal{CN}(\overrightarrow{d}_n; x_n, \overrightarrow{\sigma}_d^2)$ and $\mathcal{CN}(\overleftarrow{d}_n; x_n, \overleftarrow{\sigma}_d^2)$ are the distributions of bidirectional FS-SEs, $\eta_1 \in \mathbb{R}^+$ and $\eta_2 \in \mathbb{R}^+$ are the combination factors with $\eta_1 + \eta_2 = 1$. Assuming that the estimate variances of bidirectional FS-SEs are the same as $\overrightarrow{\sigma}_d^2 = \overleftarrow{\sigma}_d^2 = \sigma_v^2$, the output SNR of the forward FS-SE is defined as:

$$\overrightarrow{\mathrm{SNR}} = \frac{\sigma_x^2}{\sigma_v^2} \tag{23}$$

where σ_x^2 is the variance of $\mathbf{x}$. Corresponding to Equation (22), the SNR of $\overleftrightarrow{d}_n$ is written as [20]:

$$\overleftrightarrow{\mathrm{SNR}} = \frac{\mathbb{E}|\eta_1 x_n + \eta_2 x_n|^2}{\mathbb{E}|\eta_1 \overrightarrow{d}_n + \eta_2 \overleftarrow{d}_n|^2 - \mathbb{E}|\eta_1 x_n + \eta_2 x_n|^2} \approx \frac{(\eta_1 + \eta_2)^2 \sigma_x^2}{(\eta_1^2 + \eta_2^2 + 2\xi\eta_1\eta_2)\sigma_v^2} \tag{24}$$

where $\xi \in [0, 1]$ is the cross-correlation coefficient. According to the assumption that the noise of bidirectional FS-SEs is approximatively independent, i.e., $\xi \to 0$, we can obtain $\overleftrightarrow{\mathrm{SNR}} \approx \frac{1}{\eta_1^2 + (1-\eta_1)^2} \overrightarrow{\mathrm{SNR}} \geqslant \overrightarrow{\mathrm{SNR}}$. This conclusion demonstrates the performance improvement of the bidirectional combination scheme.

In fact, the noise of the bidirectional FS-SEs is not strictly independent. To acquire the property of ξ, we use the real oceanic data set of the Pengcheng Laboratory for analysis. The data set adopts binary phase shift keying (BPSK) modulation, a 10 kHz carrier frequency, 1 kSymbol/s and 40 ms LFM frame header with 8 k∼12 kHz bandwidth. The cross-correlation coefficient is calculated as [23]:

$$\xi = \frac{\overleftrightarrow{\sigma}_d^2 - \eta_1^2 \overrightarrow{\sigma}_d^2 - \eta_2^2 \overleftarrow{\sigma}_d^2}{2\eta_1\eta_2 \overrightarrow{\sigma}_d \overleftarrow{\sigma}_d} \tag{25}$$

where $\overleftrightarrow{\sigma}_d^2 = \frac{1}{N}\sum_{n=1}^{N} |\overleftrightarrow{d}_n - x_n|^2$, $\overleftarrow{\sigma}_d^2 = \frac{1}{N}\sum_{n=1}^{N} |\overleftarrow{d}_n - x_n|^2$, $\overrightarrow{\sigma}_d^2 = \frac{1}{N}\sum_{n=1}^{N} |\overrightarrow{d}_n - x_n|^2$.

We compared three kinds of situations with different fractionally spaced orders, i.e., 1/2, 1/4, 1/8. The lengths of FFF and SIC are both 20 and $\eta_1 = \eta_2 = 0.5$. Figure 5 shows that cross-correlation coefficient decreases with the fractionally spaced order. The average cross-correlation coefficients are separately 0.397, 0.311, 0.133 for the 1/2, 1/4, 1/8 fractionally spaced orders.

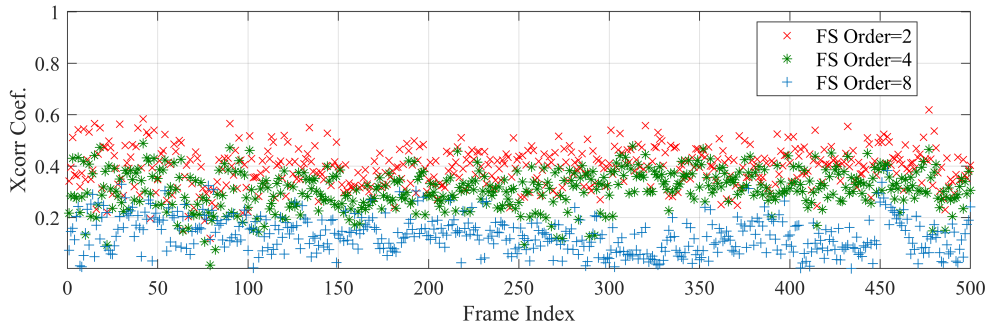

Figure 5. Estimates of cross-correlation coefficients of bidirectional FS-SEs.

3.4. Soft DA-TEQ

The soft turbo equalization utilizes the a priori soft symbol instead of hard decision feedback to the SISO equalizer, i.e., the FS-SE. For the first turbo iteration, no a priori message can be exploited for the SISO equalizer. For the later turbo iterations, the a priori probability of the SISO equalizer input symbol can be calculated by the extrinsic LLR of the MAP decoder [11], i.e., $L_{\mathrm{De}}^{\mathrm{Ext}}(\tilde{c}_n^{\dot{q}})$:

$$\begin{aligned} P(x_n = \gamma_i) &= \prod_{\dot{q}=1}^{q} P(c_n^{\dot{q}} = s_i^{\dot{q}}) \\ &= \prod_{\dot{q}=1}^{q} \frac{1}{2}\left[1 + s_i^{\dot{q}} \tanh\left(\frac{L_{\mathrm{Eq}}^{\mathrm{Pri}}(c_n^{\dot{q}})}{2}\right)\right] \end{aligned} \tag{26}$$

where $L_{\mathrm{Eq}}^{\mathrm{Pri}}(c_n^{\dot{q}})$ is the *a priori* LLR for the SISO equalizer, with $L_{\mathrm{Eq}}^{\mathrm{Pri}}(c_n^{\dot{q}}) = \prod\left[L_{\mathrm{De}}^{\mathrm{Ext}}(\tilde{c}_n^{\dot{q}})\right]$. $c_n^{\dot{q}}$ is the $\dot{q}$-th bit of the transmitted baseband symbol x_n, and $\tilde{c}_n^{\dot{q}} = \prod^{-1}\left[c_n^{\dot{q}}\right]$. We can calculate the *a priori* mean and variance of x_n [13]:

$$\bar{x}_n = \mathbb{E}\left[x_n \middle| \left\{L_{\mathrm{Eq}}^{\mathrm{Pri}}(c_n^{\dot{q}})\right\}_{\dot{q}=1}^{q}\right] = \sum_{\gamma_i \in S} \gamma_i P(x_n = \gamma_i) \tag{27}$$

$$\sigma_{x_n}^2 = \sum_{\gamma_i \in S} |\gamma_i - \mathbb{E}[x_n]|^2 P(x_n = \gamma_i) = q - |\bar{x}_n|^2 \tag{28}$$

The soft symbol $\bar{x}_n$ and $\bar{x}_{-n}$ are fed back to the bidirectional SISO equalizer for the next iteration. The equalizer error in Equation (21) is rewritten as $e_n = \bar{x}_n - \hat{d}_n$.

The conditional probability density of equalizer output symbol which assumed to follow a Gaussian distribution can be obtained by the estimated soft symbol mean value μ_d and variance σ_d^2, as [15]:

$$p(\bar{d}_n \mid x_n = \gamma_i) = \frac{1}{\pi\sigma_d^2} \exp\left(-\frac{\mid \bar{d}_n - \mu_d \gamma_i \mid^2}{\sigma_d^2}\right) \tag{29}$$

where

$$\begin{aligned} \mu_d &= \frac{1}{N}\sum_{n=1}^{N} \frac{\bar{d}_n}{Q[\bar{d}_n]} \\ \sigma_d^2 &= \frac{1}{N-1}\sum_{n=1}^{N} \mid \bar{d}_n - \mu_d Q[\bar{d}_n] \mid^2 \end{aligned} \tag{30}$$

The extrinsic LLR of the SISO equalizer is given as [16]:

$$L_{\mathrm{Eq}}^{\mathrm{Ext}}(c_n^{\dot{q}}) = \ln \frac{\sum_{\forall \gamma_i : s_i^{\dot{q}} = +1} p(\bar{d}_n \mid x_n = \gamma_i) \prod_{\forall \hat{q} : \hat{q} \neq \dot{q}} P(c_n^{\hat{q}} = s_i^{\hat{q}})}{\sum_{\forall \gamma_i : s_i^{\dot{q}} = -1} p(\bar{d}_n \mid x_n = \gamma_i) \prod_{\forall \hat{q} : \hat{q} \neq \dot{q}} P(c_n^{\hat{q}} = s_i^{\hat{q}})} \tag{31}$$

where the *a priori* probability $P(c_n^{\hat{q}} = s_i^{\hat{q}})$ is presented in Equation (26). Then, $L_{\mathrm{Eq}}^{\mathrm{Ext}}(c_n^{\dot{q}})$ is sent to the interleaver, such that the *a priori* LLR of the MAP decoder is obtained as $L_{\mathrm{De}}^{\mathrm{Pri}}(\tilde{c}_n^{\dot{q}}) = \prod^{-1}\left[L_{\mathrm{Eq}}^{\mathrm{Ext}}(c_n^{\dot{q}})\right]$. The *a posteriori* LLR of the MAP decoder, $L_{\mathrm{De}}^{\mathrm{Post}}(\tilde{c}_n^{\dot{q}})$, is produced by decoding algorithms, e.g., BJCR and soft Viterbi algorithms. We can obtain the extrinsic LLR of the MAP decoder as $L_{\mathrm{De}}^{\mathrm{Ext}}(\tilde{c}_n^{\dot{q}}) = L_{\mathrm{De}}^{\mathrm{Post}}(\tilde{c}_n^{\dot{q}}) - L_{\mathrm{De}}^{\mathrm{Pri}}(\tilde{c}_n^{\dot{q}})$. A new turbo iteration is started from Equation (26).

4. Results

4.1. Simulations

In the simulations, we concentrate on evaluating the BER performance of the proposed VSTD-TEQ compared with aspects of the fractionally spaced soft DFE-based DA-TEQ (VSD-TEQ) and soft DFE-based DA-TEQ (SDA-TEQ). Because SDA-TEQ and time-reversed structures have been proven to demonstrate significant superiority over the Hard-DA-TEQ and single direction SISO equalizer in several recent works [29,30], we do not investigate the Hard-DA-TEQ simulation here.

In the following simulations, a single-carrier SISO system with quadrature phase shift keying (QPSK) modulation is studied. The source data are thrown into a 1/2-rate RSC encoder with a generating polynomial $g = [5, 7]$ and then passed through an S-random interleaver. The coded bits are modulated in QPSK with a 10 kHz emission carrier frequency, and the symbol rate is set to 2.5 kSymbols/s. The data frame format is illustrated in Figure 6, where the transmitting signal begins with a balanced gold sequence of length N_{BG} = 1023 and ends with a frame gap of suitable length. Here we have no gap between the header and training sequence, i.e., $T_{g,1} = 0$. The balanced gold signal is applied to coarse frame synchronization and the Doppler frequency shift estimation. The lengths of the bidirectional training sequences are both 400 symbols, i.e., $N_{\mathrm{trf}} = N_{\mathrm{trb}} = 400$. The length of useful data is 1024 symbols and the gap between adjacent frames is $T_{g,2} = 100$ ms. The simulations are performed on the computer with the following specifications: AMD(R) Ryzen 7 5800H CPU 3.2 GHz (8 cores), NVIDIA(R) GeForce RTX 3070 GPU, 16 GB RAM, 2 TB memory with Windows 11 and MATLAB R2023a installed.

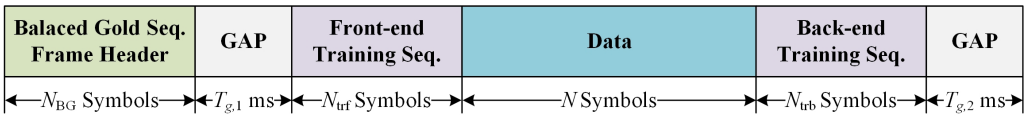

Figure 6. The frame format of transmit signal.

The UWA CIR for simulation is generated by Bellhop tools with a field collected sound speed profile of theThousand Island Lake shown in Figure 7a. As shown in Figure 7b, the depth of the transmitting transducer is 5 m with a −6 dB directivity from −5° to 90°, the depth of the receiving transducer is 15 m with a 1 km horizontal range away from the emitter. The generated CIR with the Doppler effect is demonstrated in Figure 8, where the carrier Doppler frequency shift is 5 Hz. The fractionally spaced order is 1/2 and the lengths of FFFs and SIC are 30 and 20, respectively. The $\ell_{2,0}$-PRLS algorithm is exploited to update the equalizers. In the first turbo iteration, the FS-SE degrades into the linear equalizer.

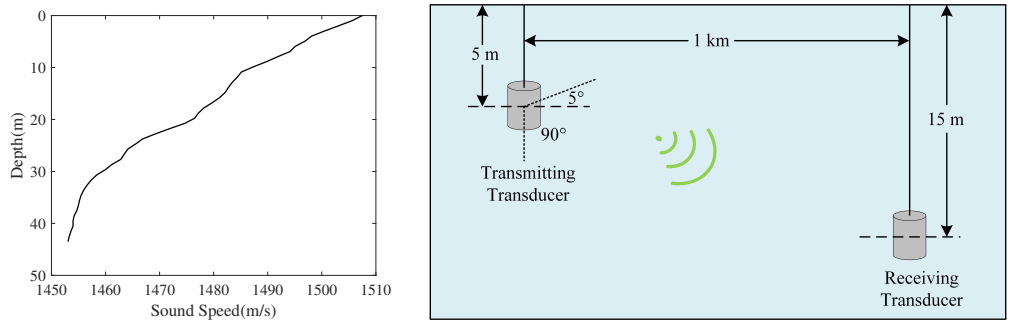

(**a**) The sound speed profile. (**b**) The experiment system implementation.

Figure 7. The environment configuration for simulation.

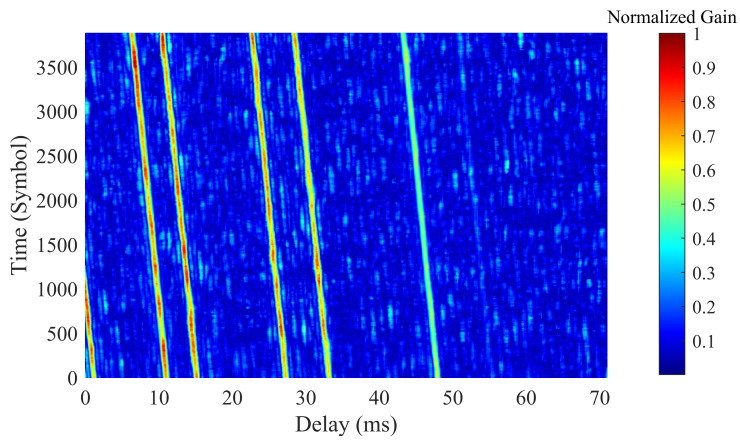

Figure 8. The CIR for simulation with Doppler effect.

The Doppler tracking curve of the first iteration is shown in Figure 9. The Doppler frequency shift is first searched cursorily using the delay-frequency search method, and the coarse capture result is 6 Hz, i.e., $\hat{a} = 6 \times 10^{-4}$, with a 2 Hz equidistant search. The average estimation of the fine Doppler frequency shift after DPLL convergence is 4.994 Hz, and the error of Doppler factor estimation attains 6×10^{-3} Hz.

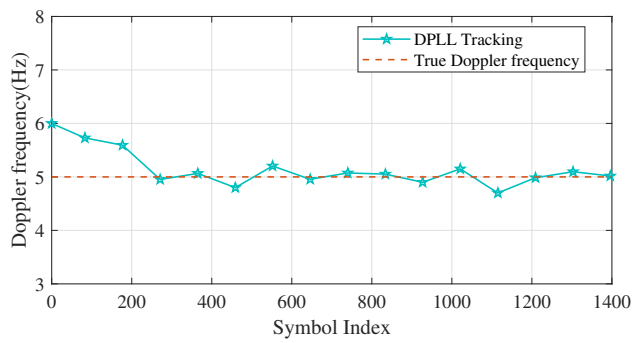

Figure 9. Doppler frequency shift tracking of DPLL (SNR = 4 dB).

The performance results are based on 1000-repetition Monte Carlo simulations. Figure 10 demonstrates the BER performance and extrinsic information transfer (EXIT) charts under the CIR simulation shown in Figure 8. Figure 10a is the BER curve comparison varying with SNR, and both the fractionally spaced structure equalizer and the bidirectional combination using virtual time-reversed technology obtain BER performance improvement. The proposed VSTD-TEQ is capable of acquiring the two-way diversity gain, which results in better BER performance, especially compared to the traditional SDA-TEQ

with a higher SNR. Figure 10b illustrates that the SISO equalizer of the proposed scheme produces superior mutual information (MI), which accelerates iteration convergence speed. Additionally, the iterative turbo equalization scheme indeed results in obvious performance amelioration for UWA communications. Moreover, the proposed scheme achieves better capacities in both BER performance and iterative convergence rates.

Table 2 shows the MMSE comparisons of different RLS-type algorithms. We can find that both the ZA and the PU methods could improve the MMSE performance for the typical RLS algorithm. As for the cluster UWA channel shown in Figure 8, the proposed $\ell_{2,0}$-PRLS has shown superior performance. For example, the $\ell_{2,0}$-PRLS algorithm has approximate 10 dB and 5 dB MMSE improvements over typical RLS and ℓ_1-PRLS, respectively.

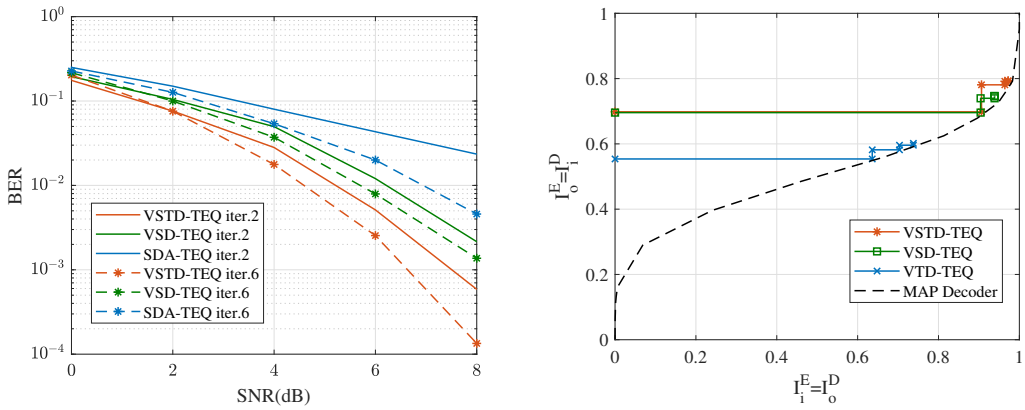

(**a**) BER curves. (**b**) EXIT charts (SNR = 4 dB).

Figure 10. Simulation results of algorithm perfromance.

Table 2. MMSE comparisons of different RLS-type algorithms.

SNR/(dB)	MMSE/(dB)				
	RLS [1]	ℓ_1-RLS [2] [29]	PRLS [3] [28]	ℓ_1-PRLS [4] [32]	$\ell_{2,0}$-PRLS [5]
5	−8.84	−9.83	−10.53	−11.01	−11.93
10	−13.99	−14.49	−15.06	−17.47	−20.10
15	−20.63	−21.72	−22.95	−24.26	−27.61
20	−25.52	−27.29	−28.23	−30.91	−35.04

[1] $\lambda = 0.995$. [2] $\lambda = 0.995, \hat{\gamma} = 2 \times 10^{-5}$. [3] $\lambda = 0.995, \tau_1 = 150, \beta_1 = 0, \tau_2 = 80, \beta_2 = 0, \epsilon_g = 10^{-9}$. [4] $\lambda = 0.995, \hat{\gamma} = 10^{-5}, \tau_1 = 150, \beta_1 = 0, \tau_2 = 80, \beta_2 = 0, \epsilon_g = 10^{-9}$. [5] $\lambda = 0.995, \hat{\gamma} = 10^{-5}, C = 4, \tau_1 = 150, \beta_1 = 0, \tau_2 = 80, \beta_2 = 0, \epsilon_g = 10^{-9}, \alpha = 2, \epsilon_p = 10^{-9}$.

4.2. Experiments

The proposed turbo equalization scheme has been verified by the real shallow-water environment with convincing conclusions. We implemented a lake trial at Huating Lake, Anhui province, China in July 2021.

For the 1500 m lake trial of SISO UWA communication, the modulation of the transmitting signal is QPSK with a constellation of $\{1+j, 1-j, -1-j, -1+j\}$. The transmission peak-to-peak voltage of the transmitting transducer is about 400 V and the equivalent electric power for transmission is approximately 40 W, caused by the internal resistance of the transducer. The carrier frequency is $f_c = 10$ kHz, and the symbol rate is set to 2.5 kSymbols/s. A 1/2-rate RSC encoder with generating polynomial $g = [5, 7]$ is adopted in a channel encoder scheme, and the S-random interleaver cooperates with the encoder. The frame formant of the transmitting signal is the same as in Figure 6; the gap between two frames is long enough to avoid inter-frame interference.

The experimental set-up of the lake trial is shown in Figure 11, where "TX" and "RX" represent the transmitter and the receiver, respectively. The transmitting system is fixed at the lake dock, and the transmitting signal is pre-generated and stored in a mobile player.

The UWA communication signal is passed from the playing device to the power amplifier, and then transmitted by an electro-acoustic transducer. The receiving system is deployed on a moving ship. The receiving ship will turn off the power and move with the water flow when it arrives at the expected experimental site. So, the receiving signal will be affected by the Doppler effect caused by the flow of water. The receiving signal from the transducer is sampled and processed in our own UWA communication modem, which is based on the DSP C6748 platform with a 456 mHz clock frequency. The decoded bit streams are sent to a PC for performance analysis and bit error rate calculation. All of the experimental data are collected and saved in the recorder. The sampling frequency of the ADC is 40 kHz, and the length of one ADC data buffer is 1500 samples. The adaptive algorithm for the equalizer adaption is based on the $\ell_{2,0}$-PRLS algorithm, which is propitious to a rapidly varying channel.

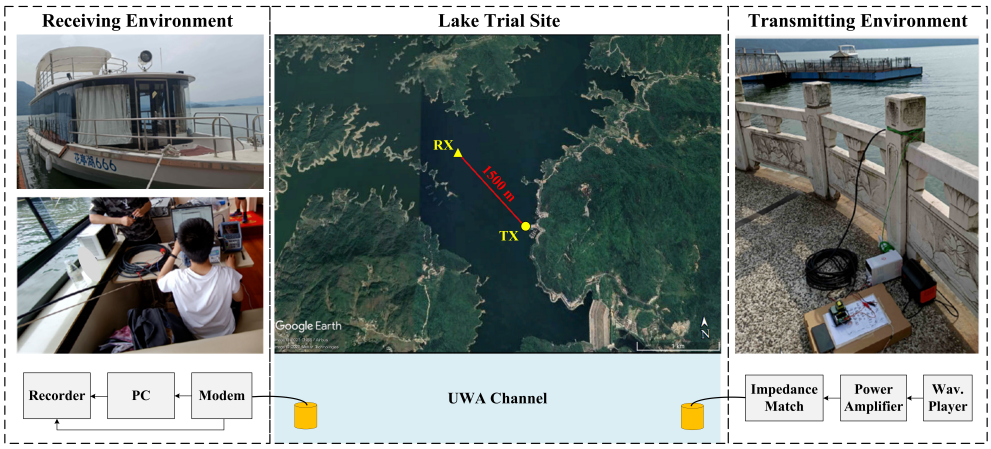

Figure 11. The experimental set-up of lake trial.

In the lake trial, a transmitting transducer is mounted at the lake wharf with 5 m depth, and a receiving transducer is tied to the experiment ship by rope, reaching about 15 m depth. The horizontal distance of the UWA communication experiment is about 1500 m, and the maximum water depth of lake trial at this time was approximately 50 m. Combined with the long and narrow terrain environment of experiment, as shown in Figure 11, we can deduce that channel multipath will be very affluent and the channel equalizer will confront potential serious challenges [6,45].

For the SISO UWA communication experiment, the signal transmission frame format and turbo receiver parameters are the same as mentioned above in the simulation section. The 1500 m received signal bursts and spectrograms collected before the ADC are shown in Figure 12 with a 400 V transmitting voltage. Apparently, the UWA signal transmission procedure suffers from serious random noise interference and harsh multipath fading. Figure 13 exhibits the estimated 1500 m CIR, and we can observe several obvious phenomena: First, the main multipath delay spread over approximately 50 ms; second, the CIR is rapidly time-varying, which makes the channel tracking even more formidable; third, the amplification gain of the receiver attains nearly 90 dB, which results in non-negligible electrical noise. The received SNR is approximately 10.08 dB.

In total, we received 88 frame signals in this trial. Figure 14 shows that the overall carrier Doppler frequency shift is within 3 Hz, and the receiving ship drifts to the transmitter during the lake trial. The frame BER results are plotted in Figure 15, where Figure 15a is the comparison result after one turbo iteration and Figure 15b is the result after four turbo iterations. For convenience, we place the frames without symbol error on the level of BER = 10^{-4}. It is obvious that the proposed VSTD-TEQ substantially outperforms the conventional SDA-TEQ and VSD-TEQ. After four turbo iterations, the number of frames involving the symbol error of the proposed VSTD-TEQ decreases rapidly, while the SDA-TEQ still retains abundant frames with detection errors.

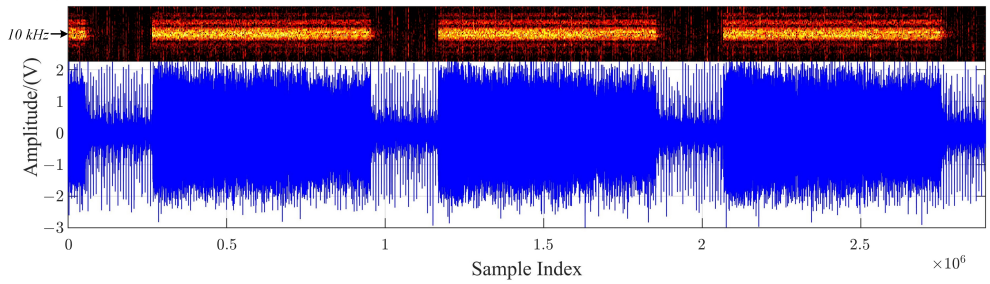

Figure 12. Example of received signals of the 1500 m lake trial.

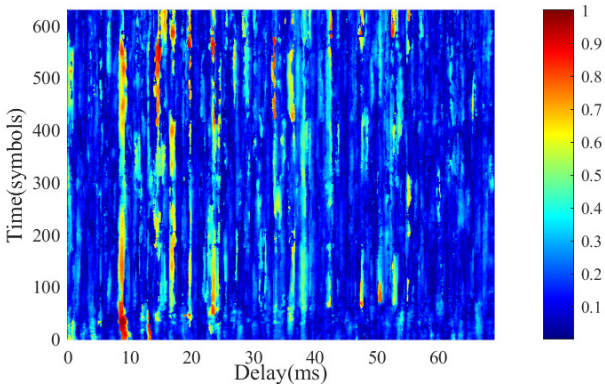

Figure 13. Estimated CIRs of the 1500 m lake trial over a period of time.

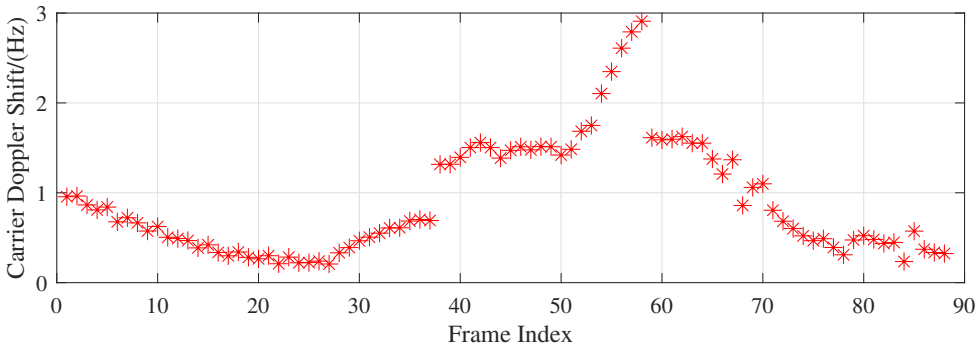

Figure 14. Estimated carrier Doppler frequency shift of 1500 m received frames (the red asterisk is the mean carrier Doppler frequency shift of one frame).

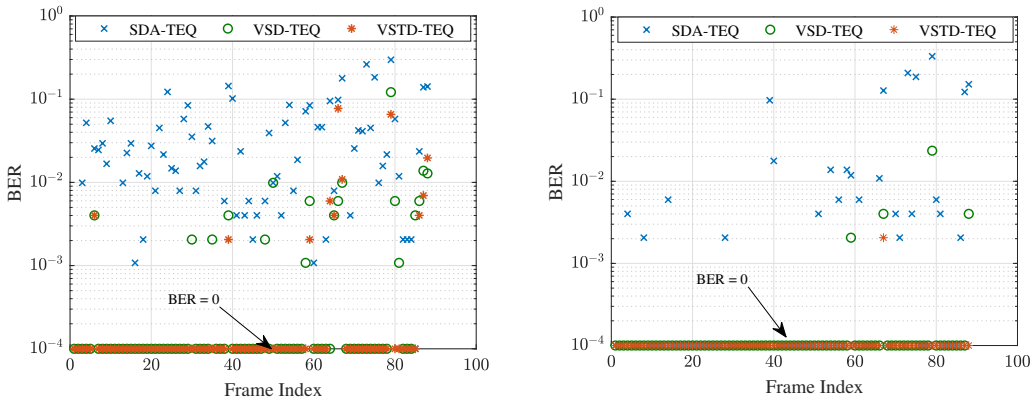

(**a**) BER comparisons of one turbo iteration. (**b**) BER comparisons of four turbo iterations.

Figure 15. Frame BER comparisons of the 1500 m lake trial.

The results of BER range comparisons are shown in Figure 16, and the BER values of 1500 m received frames are divided into several intervals. In Figure 16a, 79.55% and 87.50% of the received frames achieve zero symbol errors for the VSD-TEQ and VSTD-TEQ, respectively, after one turbo iteration. In Figure 16b, after four turbo iterations, 95.45% and 98.86% of the received frames achieve zero symbol errors for the VSD-TEQ and VSTD-TEQ, respectively. On the contrary, there are only 71.60% frames that reach BER = 0 with SDA-TEQ after four turbo iterations. Moreover, there are 6.82% frames that remain at BER $> 10^{-1}$ gradation. Apparently, the comparison results above strongly express the BER performance superiority of the proposed VSTD-TEQ over the SDA-TEQ.

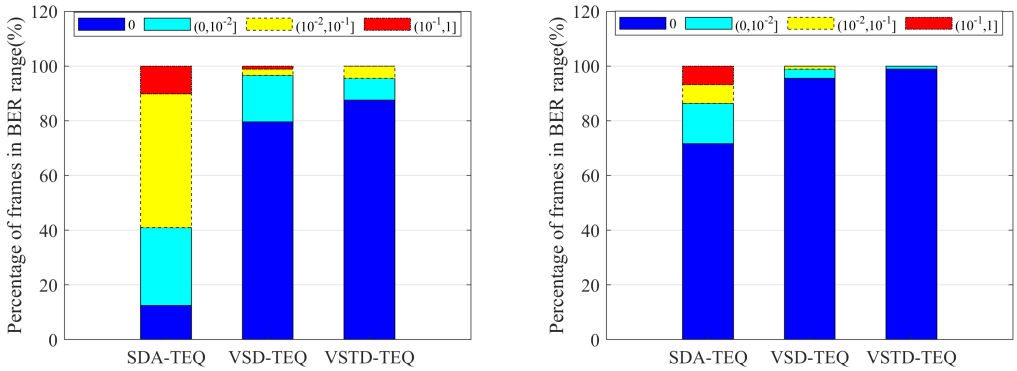

(**a**) BER range comparisons of one turbo iteration. (**b**) BER range comparisons of four turbo iterations.

Figure 16. BER range comparisons of the 1500 m lake trial.

The overall performance comparison is presented in Figure 17. In the first iteration, the MSE between the VSD-TEQ and VSTD-TEQ is almost no different. The reason for this is the absence of *a prior* information about the detection symbols. With four turbo iterations, the MSE difference attains about 5 dB between the VSTD-TEQ and the SDA-TEQ. The contribution of the fractionally spaced structure SISO equalizer is more than the bidirectional combination. In Figure 17b, the total BER of the 1500 m lake trial is decreased from 1.50×10^{-2}, with the SDA-TEQ, to 2.22×10^{-5}, with the VSTD-TEQ. The bidirectional combination sped up the convergence rate of the turbo iterations: the iterative time of convergence is only three iterations for the VSTD-TEQ, while the VSD-TEQ needs more than seven iterations.

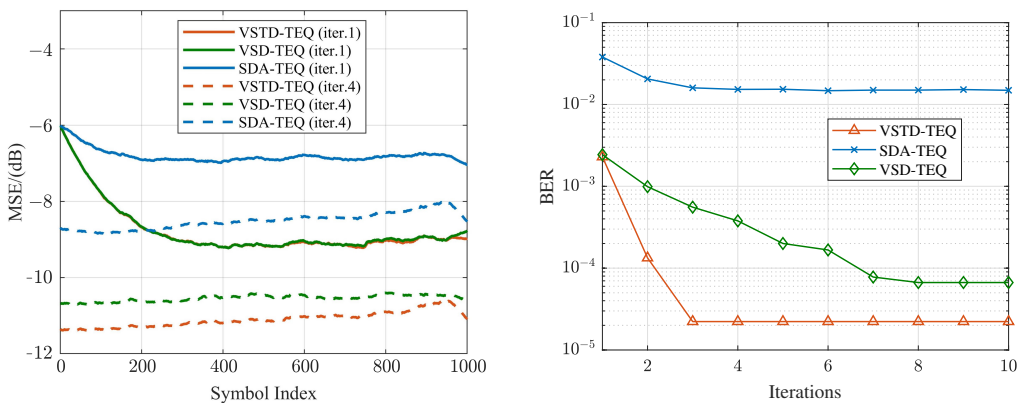

(**a**) MSE comparisons. (**b**) BER comparisons.

Figure 17. Performance comparisons of the 1500 m lake trial.

Compared with the simulation results above, the performance of the lake trial results deteriorated significantly. The reason for this is that the field channel is much more complicated corresponding to the simulations, and the comparison of UWA channels is

even more striking when observing Figures 8 and 13. The topography of the experimental site is confined and curved, so that the acoustic reflection phenomenon may occur more frequently. The summer climate is always a troublesome problem for UWA communications as it makes the acoustic propagation path difficult to predict and time-varying [46,47]. Another reason is the motion of the ship caused by waggle and water flow; thus, some propagation paths do not endure for a frame. The unstable paths may appear or disappear unexpectedly. All these facts contribute to the troublesome field channel. On the contrary, the channels generated by Bellhop have a relatively stable structure, and the simulations reflect a wide range of scenarios instead of the special experimental site.

5. Conclusions

UWA communication is one of the fundamental requirements for underwater positioning, navigation and timing networks. As for the single-carrier UWA communication, the continuous carrier phase observation from the receiver loop has the potential to provide high-precision location information in the future, just like the Beidou Navigation Satellite System. The UWA channel suffers formidable interferences caused by the underwater environment and physical acoustic characteristics. So, in this paper, we investigated the robust turbo receiving scheme of single-carrier UWA communication under harsh shallow-water channel environments, and the critical conclusions are summarized as follows:

(1) For time-varying UWA channels, the Doppler effect should be finely compensated to guarantee the stability of UWA communication. We concentrated on the fine Doppler estimation and compensation because of the low Doppler estimation accuracy demand of signal synchronization. The proposed anti-Doppler module embeds an interpolator with Farrow structure into the DPLL; thus, the cumulative timing error will be eliminated in time. To couple the ADM and equalizer effectively, we introduced the integral-zeroing module to smooth the noisy phase error. The controlling parameters of the ADM are calculated according to the output of the loop filter. Owing to the adjustable interpolator in cooperation with the DPLL, the time-scale distortion caused by the dynamic Doppler effect can be alleviated. The proposed anti-Doppler module achieves available noise reduction in phase detection, and the field lake trial verifies the reliability and robustness of the proposed scheme in time-varying UWA communication situations.

(2) To satisfy the cluster-sparse UWA channel, we considered a system transmission model with grouped multipaths. The excellent performance of the PRLS algorithm has been confirmed for sparse identification. To accelerate the convergence speed and accomplish a reduction in steady-state error, we exploited the hybrid norm regularization to rebuild the cost function of the adaptive algorithm. Combined with the proportional updating mechanism, the so-called $\ell_{p,q}$-PRLS algorithm was obtained to settle the cluster-sparse problems. Experiments have shown that the resulting $\ell_{2,0}$-PRLS algorithm presents performance superiority over existing PRLS-type algorithms in specific channels. The main drawback of the proposed adaptive algorithm is the process of parameter configuration.

(3) Turbo equalization or turbo receiver is the appropriate implementation structure to reduce the troublesome ISI for single-carrier UWA communication systems. We utilized the SIC filter to solve the noncausal interference of the channel, and the SIC should only be applied after the extrinsic soft symbols of the decoder are obtained. The improved soft FS-SE is exploited to constitute the SISO equalizer in the turbo receiver structure. To eliminate the error propagation of the feedback equalizer further, the VTRM technology is employed in our proposed VSTD-TEQ scheme. We considered that the bidirectional received baseband signals are approximatively independently identically distributed, and the experiment result demonstrated that the cross-correlation coefficient of the bidirectional input reduces along with the growth of the fractionally spaced order. In particular, the cross-correlation coefficient is approximately only 0.1, while the fractionally spaced order is 1/8,

which verifies the rationality of the bidirectional structure. Therefore, the proposed scheme is a suitable receiving implementation for fast time-varying UWA channels. The results of the simulations and the lake trial demonstrate that the proposed scheme achieves obvious MMSE and BER performance improvement over existing similar schemes.

Author Contributions: Conceptualization, Z.H. and P.J.; methodology, W.T.; software, D.Z.; validation, Z.H., W.T. and D.Z.; formal analysis, Z.H.; investigation, P.J.; resources, W.T.; data curation, W.T.; writing—original draft preparation, Z.H.; writing—review and editing, P.J.; visualization, W.T.; supervision, D.Z.; project administration, P.J.; funding acquisition, P.J. All authors have read and agreed to the published version of the manuscript.

Funding: This research was funded by the National Key Research and Development Program of China (2020YFB0505803) and National Key Research and Development Program of China (2016YFB0501700).

Institutional Review Board Statement: Not applicable.

Informed Consent Statement: Not applicable.

Data Availability Statement: Not applicable.

Conflicts of Interest: The authors declare no conflict of interest.

Abbreviations

The following abbreviations are used in this manuscript:

PNT	positioning, navigation and timing
UWA	underwater acoustic
ROV	remotely operated vehicle
AUV	autonomous underwater vehicle
UCNDIS	UWA communication, navigation and detection integration system
USBL	ultra short base line
ISI	inter-symbol interference
DFE	decision-feedback equalizer
DPLL	digital phase locked loop
BER	bit error rate
MAP	a maximum a posteriori
SISO	soft-input soft-output
MMSE	minimum mean squared error
LSER	least symbol error rate
VTRM	virtual time reversal mirror
FSE	fractionally spaced equalizer
CE-TEQ	channel-estimation-based turbo equalization
DA-TEQ	direct-adaptation-based turbo equalization
SDA-TEQ	soft DA-TEQ
LMS	least mean square
IPNLMS	improved proportional normalized LMS
MIMO	multi-input multi-output
FOLMS	fast self-optimized LMS
RLS	recursive least-squares
PRLS	proportional RLS
VSTD-TEQ	virtual space-time diversity turbo equalization
FS-SE	fractionally spaced soft interference cancellation equalizer
CIR	channel impulse response
AWGN	additive white Gaussian noise
B-CG	Bernoulli-Complex Gaussian
PSK	phase shift keying
RSC	recursive system convolutional
ADC	analog to digital converter

ADM	anti-Doppler module
SIC	soft interference cancellation
FFF	feedforward filter
FBF	feedback filters
PD	phase detector
NCO	numberically controlled oscillator
LPF	lowpass filter
LF	loop filter
EP	error propagation
EXIT	extrinsic information transfer
MI	mutual information

References

1. Zhang, T.; Han, G.; Lin, C. Integration of Communication, Positioning, Navigation and Timing for Deep-Sea Vehicles. *IEEE Netw.* **2020**, *34*, 121–127. [CrossRef]
2. Lv, C.; Shen, B.; Zhang, S. Study of Underwater Acoustic Positioning and Communication Integrated System Signal. In Proceedings of the 2022 7th International Conference on Intelligent Computing and Signal Processing (ICSP), Xi'an, China, 15–17 April 2022.
3. İnce, T.; Çakir, S. Tightly and Loosely Coupled Architectures for Inertial Navigation System and Doppler Velocity Log Integration at Autonomous Underwater Vehicles. In Proceedings of the 2022 30th Signal Processing and Communications Applications Conference (SIU), Safranbolu, Turkey, 15–18 May 2022.
4. Furfaro, T.C.; Alves, J. A communications and relative navigation architecture for underwater vehicle coordination. In Proceedings of the OCEANS 2015—MTS/IEEE Washington, Washington, DC, USA, 19–22 October 2015.
5. Parastoo, Q.; Stojanovic, M. Statistical Characterization and Computationally Efficient Modeling of a Class of Underwater Acoustic Communication Channels. *IEEE J. Ocean. Eng.* **2013**, *38*, 701–717.
6. Wu, W.; Gao, X.; Sun, C. Shallow Underwater Acoustic Massive MIMO Communications. *IEEE Trans. Signal Process.* **2021**, *69*, 1124–1139. [CrossRef]
7. Lv, Z.; Du, L.; Li, H. Influence of Temporal and Spatial Fluctuations of the Shallow Sea Acoustic Field on Underwater Acoustic Communication. *Sensors* **2022**, *22*, 5795. [CrossRef]
8. Manishika, R.; Brejesh, L.; Seshan, S. Statistical Modeling and Performance Analysis of Cooperative Communication in Frequency-Selective Underwater Acoustic Channel Using Vector Sensor. *IEEE Sens. J.* **2021**, *21*, 7367–7379.
9. Li, Z.; Stojanovic, M. Multicarrier Acoustic Communications in Multiuser and Interference-Limited Regimes. *IEEE J. Ocean. Eng.* **2023**, *48*, 542–553. [CrossRef]
10. Avrashi, G.; Amar, A.; Cohen, I. Time-varying carrier frequency offset estimation in OFDM underwater acoustic communication. *Signal Process.* **2022**, *190*, 108299. [CrossRef]
11. Tuchler, M.; Koetter, R.; Singer, A.C. Turbo equalization: Principles and new results. *IEEE Trans. Commun.* **2002**, *50*, 754–767. [CrossRef]
12. Otnes, R.; Tuchler, M. Iterative channel estimation for turbo equalization of time-varying frequency-selective channels. *IEEE Trans. Wirel. Commun.* **2004**, *3*, 1918–1923. [CrossRef]
13. Yellepeddi, A.; Preisig, J.C. Adaptive equalization in a turbo loop. *IEEE Trans. Wirel. Commun.* **2015**, *14*, 5111–5122. [CrossRef]
14. Zheng, T.; Jing, L.; Long, C. Frequency domain direct adaptive turbo equalization based on block normalized minimum-SER for underwater acoustic communications. *Appl. Acoust.* **2023**, *205*, 109266. [CrossRef]
15. Duan, W.; Tao, J.; Zheng, Y. Efficient adaptive turbo equalization for multiple-input–multiple-output underwater acoustic communications. *IEEE J. Ocean. Eng.* **2017**, *43*, 792–804. [CrossRef]
16. Xi, J.; Yan, S.; Xu, L. Soft direct-adaptation based bidirectional turbo equalization for MIMO underwater acoustic communications. *China Commun.* **2017**, *14*, 1–12. [CrossRef]
17. Rudander, J.; Paul, A.; Thor, H. Very-High-Frequency Single-Input–Multiple-Output Acoustic Communication in Shallow Water. *IEEE J. Ocean. Eng.* **2018**, *44*, 943–955. [CrossRef]
18. Xu, L.; Zhong, X.; Yu, H. Spatial and time-reversal diversity aided least-symbol-error-rate turbo receiver for underwater acoustic communications. *IEEE Access* **2018**, *6*, 9049–9058. [CrossRef]
19. Zhang, M.; Wang, Y.; Tu, X. Recursive Least Squares-Algorithm-Based Normalized Adaptive Minimum Symbol Error Rate Equalizer. *IEEE Commun. Lett.* **2023**, *27*, 317–321. [CrossRef]
20. Bozzi, F.A.; Jesus, S.M. Joint Vector Sensor Beam Steering and Passive Time Reversal for Underwater Acoustic Communications. *IEEE Access* **2022**, *10*, 66952–66960. [CrossRef]
21. Siddiqui, S.I.; Dong, H. Time Diversity Passive Time Reversal for Underwater Acoustic Communications. *IEEE Access* **2019**, *7*, 24258–24266. [CrossRef]
22. Ghassem, N.; Philippa, A.M.; Desmond, P.T. Spectral analysis of fractionally-spaced MMSE equalizers and stability of the LMS algorithm. *IEEE Trans. Commun.* **2017**, *66*, 1675–1688.

23. Xi, J.; Yan, S.; Xun, L. Sparsity-Aware Adaptive Turbo Equalization for Underwater Acoustic Communications in the Mariana Trench. *IEEE J. Ocean. Eng.* **2021**, *46*, 338–351. [CrossRef]
24. Liang, Y.; Yu, H.; Ji, F. Multitask Sparse Bayesian Channel Estimation for Turbo Equalization in Underwater Acoustic Communications. *IEEE J. Ocean. Eng.* **2023**, *48*, 946–962. [CrossRef]
25. Qin, X.; Qu, F.; Zheng, Y. Bayesian Iterative Channel Estimation and Turbo Equalization for Multiple-Input-Multiple-Output Underwater Acoustic Communications. *IEEE J. Ocean. Eng.* **2021**, *46*, 326–337. [CrossRef]
26. Qin, X.; Diamant, R. Joint Channel Estimation and Decoding for Underwater Acoustic Communication with a Short Pilot Sequence. *IEEE J. Ocean. Eng.* **2023**, *48*, 526–541.
27. Meng, Q.; Huang, J.; Han, J. An improved direct adaptive multichannel turbo equalization scheme for underwater communications. In Proceedings of the Oceans 2012—Yeosu, Yeosu, Republic of Korea, 21–24 May 2012.
28. Qin, Z.; Tao, J.; Han, X. Sparse direct adaptive equalization based on proportionate recursive least squares algorithm for multiple-input multiple-output underwater acoustic communications. *J. Acoust. Soc. Am.* **2020**, *148*, 2280–2287. [CrossRef]
29. Liu, L.; Zhang, Y.; Sun, D. VFF l_1-norm penalised WL-RLS algorithm using DCD iterations for underwater acoustic communication. *IET Commun.* **2017**, *11*, 615–621. [CrossRef]
30. Tao, J.; Wu, Y.; Han, X. Sparse direct adaptive equalization for single-carrier MIMO underwater acoustic communications. *IEEE J. Ocean. Eng.* **2019**, *45*, 1622–1631. [CrossRef]
31. Zhang, Y.; Zakharov, Y.; Li, J. Soft-decision-driven sparse channel estimation and turbo equalization for MIMO underwater acoustic communications. *IEEE Access* **2018**, *6*, 4955–4973. [CrossRef]
32. Qin, Z.; Tao, J.; Xia, Y.; Le, Y. Proportionate RLS with l_1 norm regularization: Performance analysis and fast implementation. *Digit. Signal Process.* **2022**, *122*, 103366. [CrossRef]
33. Qin, Z.; Tao, J.; Tong, F.; Zhang, H. A fast proportionate RLS adaptive equalization for underwater acoustic communications. In Proceedings of the OCEANS 2019—Marseille, Marseille, France, 17–20 June 2019.
34. Liu, Z.; Bai, F.; Song, L. Underwater decode-interleave-forward cooperative strategy for underwater acoustic communication. *IEEE Access* **2019**, *7*, 19698–19708. [CrossRef]
35. Yan, L.; Ma, X.; Li, X. Shot Interference Detection and Mitigation for Underwater Acoustic Communication Systems. *IEEE Trans. Commun.* **2021**, *69*, 3274–3285. [CrossRef]
36. Roy, S.; Duman, T.; McDonald, V. High-rate communication for underwater acoustic channels using multiple transmitters and space–time coding: Receiver structures and experimental results. *IEEE J. Ocean. Eng.* **2007**, *32*, 663–688. [CrossRef]
37. Wang, S.; Liu, M.; Li, D. Bayesian learning-based clustered-sparse channel estimation for time-varying underwater acoustic OFDM communication. *Sensors* **2021**, *21*, 4889. [CrossRef] [PubMed]
38. Sun, D.; Hong, X.; Cui, H.; Liu, L. A Symbol-Based Passband Doppler Tracking and Compensation Algorithm for Underwater Acoustic DSSS Communications. *J. Commun. Inf. Netw.* **2020**, *5*, 168–176. [CrossRef]
39. Shen, L.; Benjamin, H.; Zakharov, Y.; Mitchell, P. Digital Self-Interference Cancellation for Full-Duplex Underwater Acoustic Systems. *IEEE Trans. Circuits Syst.* **2020**, *67*, 192–196. [CrossRef]
40. Jiang, P.; Shi, C.; Wu, M. Simulations of code and carrier loop by Farrow interpolation in BD Navigation System. *Geomat. Inf. Sci. Wuhan Univ.* **2009**, *34*, 548–551.
41. Qiao, G.; Zhao, Y.; Liu, S. Doppler scale estimation for varied speed mobile frequency-hopped binary frequency-shift keying underwater acoustic communication. *J. Acoust. Soc. Am.* **2019**, *146*, 998–1004. [CrossRef]
42. Pelekanakis, K.; Chitre, M. Robust equalization of mobile underwater acoustic channels. *IEEE J. Ocean. Eng.* **2015**, *40*, 775–784. [CrossRef]
43. Riedl, T.; Singer, A. MUST-READ: Multichannel sample-by-sample turbo resampling equalization and decoding. In Proceedings of the 2013 MTS/IEEE OCEANS—Bergen, Bergen, Norway, 10–14 June 2013.
44. Li, Y.; Jiang, Z.; Jin, Z.; Han, X.; Yin, J. Cluster-Sparse Proportionate NLMS Algorithm with the Hybrid Norm Constraint. *IEEE Access* **2018**, *6*, 47794–47803. [CrossRef]
45. Pelekanakis, K.; Blouin, S.; Green, D. Performance Analysis of Underwater Acoustic Communications in Barrow Strait. *IEEE J. Ocean. Eng.* **2021**, *46*, 1438–1449. [CrossRef]
46. Liu, Y.; Chen, Y.; Meng, Z. Performance of single empirical orthogonal function regression method in global sound speed profile inversion and sound field prediction. *Appl. Ocean Res.* **2023**, *136*, 103598.
47. Yan, Z.; Yang, X.; Sun, L. Inter-carrier interference-aware sparse time-varying underwater acoustic channel estimation based on fast reconstruction algorithm. *China Commun.* **2021**, *18*, 216–225. [CrossRef]